Egypt. J. Chem. **Vol. 68**, No. 12 pp. 107 - 128 (2025)

Egyptian Journal of Chemistry

http://ejchem.journals.ekb.eg/

Design, Characterization, Analytical, Computational, Antibacterial and Mechanistic Behavior of Novel Copper(II) Schiff Base Nano-Complex

Anas H. Abdel-rahman, Elsayed RH El-Gharkawy, Ghada E. Abdel-Ghani and Magda A Akl*

Chemistry Department, Faculty of Science, Mansoura University 35561, Mansoura, Egypt

Abstract

3-acetylcoumarin thiosemicarbazone was investigated as a Schiff base ligand (L_1) for the synthesis of a copper(II) complex. The ligand (L_1) and its copper(II) Schiff base nano-complex were characterized by Fourier transform infrared spectroscopy (FTIR), Transmission electron microscopy (TEM), Ultraviolet-Visible spectroscopy (UV–Vis), and elemental analysis. The Schiff base nano-complex [Cu(II)-(L_1)] was effectively separated by flotation using oleic acid (HOL) as an anionic surfactant. Flame atomic absorption spectrometry (FAAS) was used to quantify Cu(II) ion content in various pharmaceutical and environmental samples, including synthetic mixtures. Experimental variables affecting the flotation process such as pH, the concentration of metal ions, ligand, HOL, temperature, and interfering ions were investigated. The analytical detection limit of Cu(II) was 0.052 mgL^{-1} with a pre-concentration factor of 125. The recovery (%) of Cu(II) was almost 100% and the relative standard deviation (RSD %) was 0.3869. The flotation mechanism is also elucidated. Moreover, the antimicrobial efficacy of the synthesized ligand (L_1), along with its copper(II) Schiff base nano-complex was examined against Gram-negative and Gram-positive bacterial strains. Additionally, computational and theoretical investigations were conducted to rationalize the experimental work and support the obtained results. The Gaussian 09 program package was used to perform the computational analyses for this investigation. Based on the experimental results, a flotation mechanism was proposed.

Keywords: Schiff base, coumarin, thiosemicarbazone, DFT, ESP, FAAS, and biological activity.

1. Introduction

The worldwide availability of potable water for human consumption represents a critical and pervasive issue given its direct consequences for both ecological systems and human well-being [1]. The ongoing expansion of industrial activities has prompted numerous investigations on the treatment of industrial byproducts. A primary concern in water pollution stems from heavy metal ions, which constitute a significant category of industrial wastes. These ions, including copper, palladium, mercury, cobalt, and cadmium, are well-documented for their toxicity and carcinogenic properties. [2]. At present, the attention to the problems of contamination by heavy metals is constant, from the point of view of finding materials with the capacity to remove metals and in the optimization of known processes [3].

The extensive industrial use of copper and its compounds has resulted in numerous potential sources of copper pollution [4]. This metal ion holds a distinctive position among the various ions essential for biological functions. Its critical importance is evident in multiple areas, including the cellular respiration process, the blood of invertebrates, and the formation of hemocyanin molecules [5]. The unique properties of ions make them indispensable in these biological contexts. The widespread application of copper in metallurgical and chemical industries has led to an increased interest in this element. Copper also plays a vital role in maintaining myelin integrity within the nervous system. In addition to these functions, copper is essential for numerous other critical physiological processes [6].Therefore, it is to isolate and quantify copper from other elements. Environmental and biological samples often contain heavy metals in trace amounts, and their analysis can be hindered by interfering substances. Consequently, before measurement, it is typically necessary to employ a technique to concentrate and isolate the target elements. With this aim in mind, a diverse set of analytical methodologies has been utilized, such as (GFAAS) graphite flame atomic absorption spectrometry [7-9], activated carbon adsorption [10,11], precipitation [12], LLE (liquid-liquid extraction) [13], Adsorption [14- 20], column extraction [21], ISE (ion-selective electrode) [22], CPE (cloud point extraction) [23], and flotation [24,25].

The "Green Chemistry" principles have made flotation a subject of significant interest [26]. This method is widely utilized for detecting trace amounts of heavy metals in various media [27]. Flotation offers numerous advantages, including simplicity, speed, cost-effectiveness, low residual metal concentrations, minimal space requirements, and versatility in applications for different metals at varying levels [28]. This technique involves using surfactants to make ionic metal species in wastewater water-repellent, and then eliminating these hydrophobic components through the application of air bubbles [29]. This technique capitalizes on the differences in surface characteristics, particularly wettability, to differentiate between

*Corresponding author e-mail: magdaakl@yahoo.com.; (Magda A Akl).
Received date 13 January 2025; Revised date 25 March 2025; Accepted date 18 April 2025
DOI: 10.21608/ejchem.2025.351125.11160

particle types. Hydrophobic particles are extracted from the aqueous phase by attaching to rising air bubbles, which accumulate in the scum layer on the surface. This layer was then harvested, and the concentrated hydrophobic particles were either used directly or subjected to further processing [30].

The ligand 3-acetylcoumarin thiosemicarbazone (L1) and other heterocyclic substances have become the focus of extensive research due to their multifaceted potential. Coumarins, a significant class of oxygen-containing heterocycles derived from benzopyrones, are abundant in various plants. The coumarin nucleus (2H-1-benzopyran-2-one) is fundamental to the chemical makeup of both natural and synthetic products [31]. Thiosemicarbazones, which contain nitrogen, oxygen, and sulfur donor atoms, are essential chelating ligands with pharmacological properties. These compounds effectively chelate transition metals, and their metal complexes exhibit a wide array of activities [32]. Molecular hybridization, which combines two physiologically significant scaffolds such as coumarins and thiosemicarbazides, can enhance the pharmacological attributes of the resulting compounds. Molecules containing the coumarin moiety and its derivatives have been linked to numerous biological applications, including antibacterial, anti-inflammatory, antiviral, antioxidant, anticancer, and antibiotic properties [33].

To overcome copper pollution problems, the ligand 3-acetylcoumarin thiosemicarbazone (L_1) has been utilized to preconcentrate Cu(II) ions using a flotation technique.

According to a survey of the literature, it was found that the ligand and its derivatives made complexes with metal ions including Cu(II) metal ions, but there is no data based on the preconcentration of Cu(II) using the flotation-FAAS technique. Additionally, there is no information on DFT analyses of the ligand (L_1) alone or along with its copper(II) Schiff base nano-complex.

Drawing from the previously mentioned details, the aims of this research can be outlined as follows: i. synthesis and characterization of a Cu(II) Schiff base nano-complex, utilizing 3-acetyl coumarin thiosemicarbazone as the Schiff base ligand; ii. employing Flotation-FAAS for ultra-trace detection of Cu(II) in diverse pharmaceutical and environmental samples, as well as synthetic mixtures; iii. examining the experimental factors that influence separation efficiency, such as pH, surfactant concentration, metal ion and chelating ligand concentrations, temperature, and the impact of foreign ions; iv. assessing the biological activity of both the ligand (L_1), along with its copper(II) Schiff base nano-complex, with findings indicating that the ligand (L_1), along with its copper(II) Schiff base nano-complex showed potent bactericidal properties when tested on S. aureus and E. coli; v. conducting DFT studies on the ligand (L_1), and its copper(II) Schiff base nano-complex to provide a theoretical basis for the investigative studies and corroborate the procured results; vi. clarifying the potential mechanism of flotation of Cu(II) Schiff base nano-complex using the HOL surfactant.

2. Experimental

2.1. Materials and solutions

This research exclusively employed analytical reagent-grade substances or those with the highest attainable purity. Double-distilled water (DDW) was used to make aqueous solutions. To prepare an oleic acid (HOL) stock solution (6.36×10^{-2} $molL^{-1}$), food-grade HOL (20 mL) (sp. gr. 0.895) was dissolved in one liter of kerosene provided by J.T. Baker Chemical Co. A stock solution of the Schiff base ligand (L_1) (1×10^{-3} $molL^{-1}$) was prepared by dissolving 0.026 g (L_1) in 60 mL of ethanol and 40 mL distilled water. Copper(II) chloride-dihydrated $CuCl_2.2H_2O$ was obtained from Sigma-Aldrich. Different stock solutions were then prepared. 1.5×10^{-3} $molL^{-1}$ Cu(II) was prepared by dissolving 0.0268 g of $CuCl_2.2H_2O$ in 100 mL of DDW in the presence of 1.0 mL HCl (conc).

2.2. Instrumentation

The flotation cells used in this study have previously been described [34]. Flotation cell (a) is a cylindrically graduated glass tube of 16 mm inner diameter and 290mm length with a stopcock at the bottom. The other design, flotation cell (b), was a cylindrical tube measuring 45 cm in length and 6 cm in internal diameter, featuring a stopcock at the bottom and a quick-fit stopper at the upper end. pH adjustments were carried out using a Hanna Instruments digital pH meter (model 8519). Elemental analyses (C, H, N, S) were performed on NC Soil Analyzer Flash 2000. A JASCO FT/IR-460 spectrophotometer, operating in the 450-4000 cm^{-1} range, was employed to analyzethe ligand and its solid-state isolated complex. The particle size of the [Cu(II)-(L_1)] complex was measured using Transmittance electron microscopy, (JEOL JEM-2100). UV-Vis spectra of the ligand (L_1), along with its copper(II) Schiff base nano-complex (C_1) were acquired using a Perkin Elmer 550 spectrophotometer with a 1cm quartz cell in ethanol (200-900 nm range). A Perkin Elmer 2380 flame atomic absorption spectrometer was used to analyze Cu(II)at 324.8 nm.

2.3. Preparations

2.3.1. Preparation of 3-Acetylcoumarin

Refluxing (2 mL) ethyl acetoacetate and (2 mL) salicylaldehyde in absolute EtOH (20 mL) in the presence of piperidine (0.5 mL) for 4h to produce pale yellow power precipitate with m.p = 120 °C. After filtering out the precipitate, it was cleaned with EtOH and then recrystallized [35].

The optical image of the formed 3-acetylcoumarin is presented in **Fig. S1**.

2.3.2. Preparation of ligand 3-Acetylcoumarin thiosemicarbazone (L_1)

Refluxing thiosemicarbazide (0.01 mole) with a 30 mL of 3-acetylcoumarin (0.01 mole), and acetic acid (3 mL) for 3 h to produce golden yellow crystals precipitate with yield of 86% and m.p = 220 °C. After filtering out the precipitate, it was

cleaned with EtOH and then recrystallized [36]. The optical image of the ligand is presented in **Fig. S2**. **Scheme 1** shows the proposed mechanism of synthesis of Schiff base ligand (L_1) and the 3D structure of (L_1) is presented in **Scheme 2.**

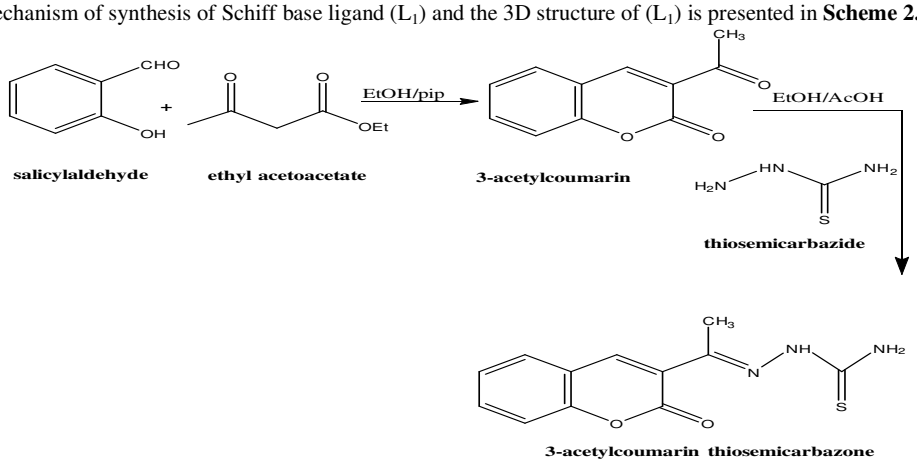

Scheme 1: Synthesis of ligand 3-Acetylcoumarin thiosemicarbazone (L_1)

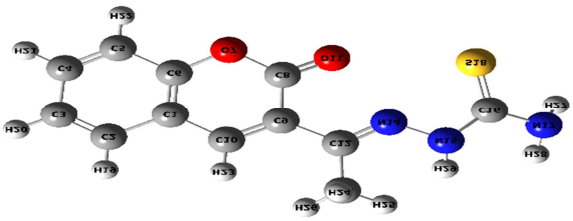

Scheme 2: 3D structure of ligand

2.3.3. Preparation of [Cu(II)-(L_1)] complex (C_1)

The synthesis of the copper Schiff base nano-complex (C_1) involved combining $CuCl_2.2H_2O$ (10.0 mmole, 0.017g) in 10 mL of DDW with an equal volume of ligand (L_1). This mixture was refluxed for 6 hours at 100 °C, resulting in a deep brown precipitate. The product was then isolated through filtration, thoroughly washed with a water/ethanol solution, and subsequently dried under vacuum conditions.

2.4. Procedure

2.4.1. Flotation- separation of Cu(II)

For the separation and determination of copper a suitable known amount (7.87×10^{-5} molL^{-1}) of Cu(II) was mixed with 2.5 mL (2×10^{-4} molL^{-1}) of the ligand with addition of 5.0 mL of DDW. The solution's pH was then adjusted to 5 using 2 mL of acetate buffer (0.1 molL^{-1} acetic acid and 0.1 molL^{-1} sodium acetate). This mixture was subsequently transferred to a flotation cell and brought to a total volume of 10 mL using DDW. A brief agitation of the cell facilitated complex formation, resulting in instant yellow discoloration of the Cu(II) Schiff base nano-complex, **Fig. 1c**. Following this, 2 mL of $2x10^{-4}$ molL^{-1} HOL was introduced to the flotation cell. The cell underwent manual shaking for 1 minute, followed by vigorous agitation in the presence of the surfactant (HOL). This process produced air bubbles, which improved the floatability of the metal/ligand complex. After reaching equilibrium, a scum layer developed, rendering the watery solution colorless, **Fig. 1d**. The scum layer was eluted using 2 mL of 1.0 molL^{-1} HNO_3. The eluted solution was delivered to the flame and the concentration of Cu(II) was measured at 324.8 nm. The flotation efficiency (F%) was calculated using **Eq. 1**.

$F\% = (C_f/C_i) \times 100$ (1)

In this equation, C_i represents the analyte's initial concentration in the aqueous layer prior to flotation, while C_f denotes the analyte's concentration in the scum layer following the flotation process.

A different approach for determining the Cu(II) flotation effectiveness (F%) can be derived from **Eq. 2.**

$F\% = (C_i-C_f) / Ci \times 100\%$ (2)

Where C_i is the initial concentration of analyte before flotation and C_f is the analyte concentration in the mother liquor after flotation.

A calibration curve spanning concentrations from 1.0 to 9.0 µg/mL was established. The concentration of Cu(II) ions was subsequently measured using flame atomic absorption spectroscopy (FAAS) with readings taken at 324.8 nm.

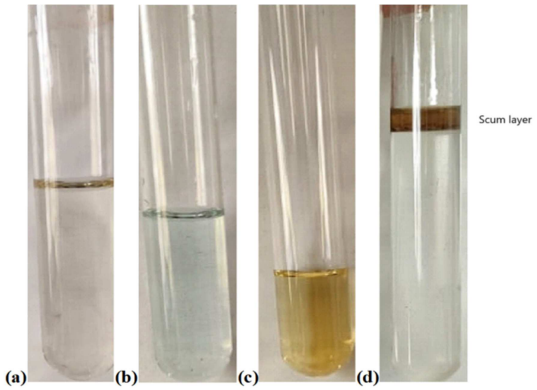

Figure 1:(a) solution of L_1, **(b)** Cu(II) solution, **(c)** [Cu(II)-(L_1)] in aqueous solution, and **(d)** scum layer containing the floated [Cu(II)-L_1] complex.

2.4.2. Analysis Water samples and pharmaceutical drugs

Several natural water samples, including distilled water, Nile water, tap water, and seawater, were collected from Al-Mansoura and Marsa-Matrouh cities. Before analysis, the water samples were pre-filtered, the pH was set to 1.0 by concentrated HCl drops, and they were kept in clean, high-quality plastic containers.

The analysis of copper content was conducted using two pharmaceutical tablet samples containing copper available in the Egyptian market: Totavit tablet (Egyphar company) which contains Vitamins along with a very important trace element (0.9 mg of copper) and Vitastress tablet (Medical Union Pharmaceuticals) multivitamins and minerals (3 mg of copper). To prepare these samples for examination, a specific dissolution technique was implemented. Each tablet underwent separate treatment with concentrated nitric acid. The process involved dissolving one pill of each tablet in 5 mL of concentrated HNO_3 individually. The resulting solutions were then carefully transferred to 50 mL volumetric flasks. These flasks were subsequently filled to the designated mark with double-distilled water (DDW). Following this preparation, the samples were subjected to copper analysis using the recommended general procedure [37].

2.5. Theoretical and computational methods

DFT calculations, encompassing geometry optimizations, were conducted on the ligand (L_1) and its corresponding Cu(II) Schiff base nano-complex. DFT is viewed as an economical approach for estimating the effects of electron correlation. The B3LYP level of theory was employed for all density functional theory (DFT) computations. This approach combines Becke's three-parameter (B3) nonlocal exchange with the Lee, Yang, and Parr (LYP) correlation functional [38]. Currently, the B3LYP level is extensively employed in the study of organic electronic compounds due to its reliable prediction of molecular geometries and accurate estimation of HOMO-LUMO gaps, which align well with experimental results [39 - 44]. The B3LYP level calculations were performed using the DGDZVP basis set for all atoms. DGDZVP, which stands for Density Gauss Double-Zeta with Polarization functions, is classified as a complete electron basis set. It incorporates 36 basis functions and 114 Gaussian primitive functions, specifically optimized for density functional theory (DFT) methods [45,46]. The Gaussian09 software package [47] was employed to perform all computations using the B3LYP/DGDZVP level of theory for every atom. The GaussSum2.2.5 program [48] was utilized to generate IR spectra, while comprehensive natural bond orbital (NBO) analyses were conducted to determine charge distribution across all molecules using NBO version 3.1 [49]. Various graphical representations of molecular shapes and distinct molecular orbitals were obtained through the Gauss View 5.0 package [50].

The Highest Occupied Molecular Orbitals (HOMO) and Lowest Unoccupied Molecular Orbitals (LUMO) represent critical aspects in the field of theoretical molecular design [51]. According to Koopman's theorem [52], the energies of the HOMO and LUMO orbitals can be utilized to determine various electronic properties and reactivity descriptors. These include electronegativity (χ), ionization potential (IP), hardness (η), electron affinity (EA), and softness (σ), which are crucial in understanding the electronic behavior and reactivity of molecules.

Table 1: Global Reactivity Descriptors (GRD)

GRD	Equation
The energy gap (ΔE_{gap})	$\Delta E_{gap} = (E_{LUMO} - E_{HOMO})$
Softness (σ)	$\sigma = \frac{1}{\eta}$
Electron affinity (E_A)	$E_A = - E_{LUMO}$
Ionization potential (I_P)	$I_P = - E_{HOMO}$
Hardness (η)	$\eta = \frac{I_P - E_A}{2}$
Chemical potentials (μ)	$\mu = - \chi$

Electronegativity (χ)	$\chi = \frac{I_P + E_A}{2}$
Electrophilicityindex (ω)	$(\omega) = \frac{\mu^2}{2\eta}$
The Global electrophilicity index (ω)	$= \frac{\mu^2}{2\eta}$
Electronic chemical potential [58] (μ)	=- Electronegativity = $\mu = -\chi$
The back donation	$(\Delta E_{back\text{-}donation}) = -\frac{\eta}{4}$

2.6. Antimicrobial studies

Similar to the disk-diffusion method, the agar plate surface is inoculated by spreading a volume of the microbial inoculum over the entire agar surface. The investigation centered on two bacterial types: Gram-positive organisms, specifically *S. aureus*, and Gram-negative microbes, namely *E. coli* which were obtained from Mansoura University Center of Genetic Engineering and Biotechnology. The antibiotics used are Ciprofloxacin (CIP), Amoxicillin (AX), and Gentamycin (GN) with *E. coli* and Ampicillin s. (A/S), Ceftazidine (CAZ), and Cefotaxime (CTX) with *S. aureus*. Next, using a sterile cork borer or tip, a hole of 6 to 8 mm in diameter is aseptically punched. The well is then filled with 100 µL of the ligand (L_1), along with its copper(II) Schiff base nano-complex at the proper concentration. After that, agar plates are incubated at the appropriate conditions based on the test microorganism. As it permeates the agar media, the antimicrobial ingredient stops the bacteria growth [59,60].

3. Results and Discussion

3.1. Method development

The optimized parameters of FAAS are given in **Table 2**.

Table 2: Optimal parameters of FAAS for determining Cu(II).

Parameter	Cu(II)
Wavelength (nm)	324.8
Lamp current [%]	100
Time of measurement [sec.]	3
Sensitivity [mg/dm^3]	0.045
Concentration of standard solutions [mg/cm^3]	2,4,5
Spectral width slit [nm]	0.7
Acetylene flow rate [dm^3/min]	0.8-1.0
Background correction	Off

3.2. Characterization

3.2.1. FTIR spectra

Fig. 2 demonstrates the FTIR spectrumof the ligand (L_1), the [Cu(II)-(L_1)] complex in the aqueous layer, and [Cu(II)-(L_1)] complex in the scum layer (HOL).

FTIR spectrum of ligand (L_1)

Fig. 2a, shows the spectrumof the ligand which exhibits absorption bands at 3381, (3235- 3147), and 3039 cm^{-1} which can be recognized to the ν(NH), ν(NH_2), and ν(C=C), respectively. The sharp bands at 1711, 1600, and 1362 cm^{-1} which can be assigned to bands ν(C=O), ν(C=N), and ν(C=S), respectively [61].

FTIR spectrum of the [Cu(II)-(L_1)] complex in aqueous phase

The complexation of the ligand with Cu(II) ion is demonstrated by the IR spectra of the[Cu(II)-(L_1)]complex shown at **Fig. 2b,** the infrared (IR) spectroscopy results demonstrate that the ligand (L_1) has formed a complex with the metal ion. This is evident when comparing the spectrum of the complexed ligand to that of (L_1) in its unbound state, the IR of the Schiff base nano-complex (C_1) shows disappearance of ν(NH) band and the band of ν(NH_2) appear in the broad band in the range of (3570-3088) cm^{-1} . the band of ν(NH_2) appear broad due to solvent of ethanol. While there is a shift in bands ν(C=O), ν(C=N), and ν(C=S) as the bands appear at 1719, 1608, and 1382 cm^{-1} respectively. On the other hand, the newly discovered bands at 597, 535, and 483 cm^{-1} and regions attributed to ν(Cu-O), ν(Cu-N), and ν(Cu-S) respectively [62].

From IR spectra it was detected that the ligand manages as monobasic tridentate ligand, coordinating through ketonic oxygen, azomethine nitrogen through coordination bond, and thiolic sulfur through covalent bond while the carbonyl of lactone and –NH_2 remain free.

Scheme 3 shows the proposed mechanism of [Cu(II)-(L_1)] complex (C_1) preparation and **Scheme 4** shows the 3D structure of the complex.

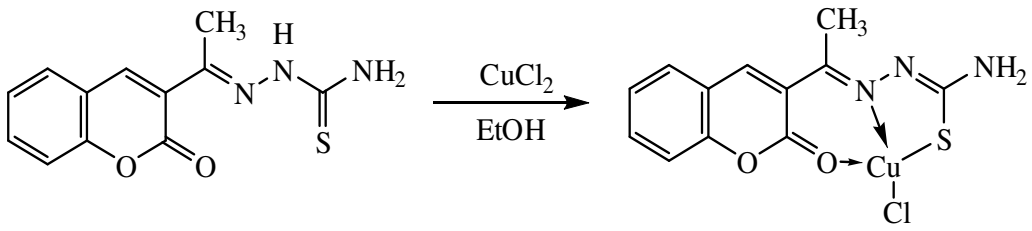

Scheme 3: Synthesis of copper(II) thiosemicarbazone complex

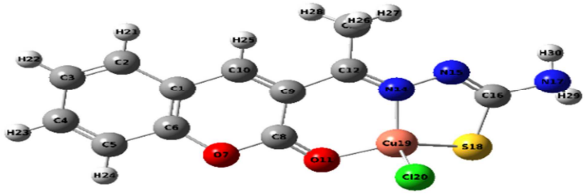

Scheme 4: 3D Structure of Cu(II) complex

FTIR spectra of the [Cu(II)-(L_1)] complex in the scum layer(HOL)

The IR spectrum of the copper Schiff base nano-complex formed in the oleic acid layer is illustrated in **Fig. 2c**. The infrared spectra of the complex isolated in the scum layer is completely different from the aqueous layer. The [Cu(II)-(L_1)] complex in the scum layer has absorption bands corresponding to the oleic acid surfactant at 2856 and 2925 cm^{-1}, corresponding to symmetric and asymmetric -CH_2 stretches, respectively. An intense band at 1707 cm^{-1} was attributed to the asymmetric -C=O stretch, while the band at 1285 cm^{-1} was linked to the C-O stretch. Furthermore, bands observed at 1464 and 939 cm^{-1} were determined to represent the in-plane and out-of-plane O-H stretches, respectively [63,64].

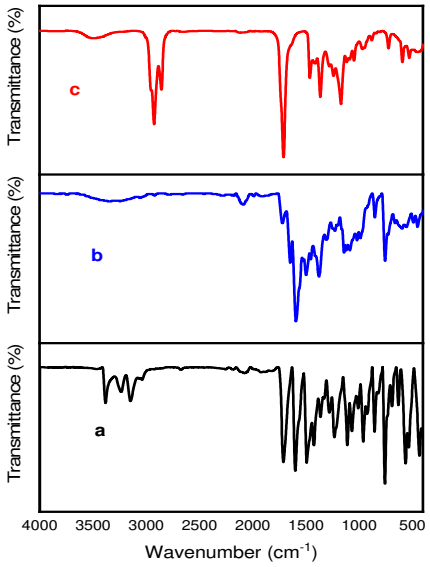

Figure 2: the FTIR spectra of **(a)** ligand L_1, **(b)** [Cu(II)-(L_1)] complex in the aqueous layer, and **(c)** [Cu(II)-(L_1)] complex in the scum layer (HOL).

3.2.2. UV-vis spectra

Fig. 3 indicates the electronic absorption spectra of ligand (L_1), and [Cu(II)-(L_1)] Schiff base nano-complex in an aqueous solution and HOL (scum layer). As seen in **Fig. 3a**, the ligand expresses one absorption bands at 249 nm which was determined to be the result of intra-ligand charge transfer (π-π* and n- π*). **Fig. 3b** exhibits two absorption bands at 249 and 394 nm which are the two absorption bands of the [Cu(II)-(L_1)] in an aqueous solution. These additional absorption bands result from electronic transitions within the d-orbitals of transition metal ion in the complex. The [Cu(II)-(L_1)] complex in the scum layer exhibits bands at 250, 442 and 910 nm as shown at **Fig. 3c.** The absorbance value of [Cu(II)-(L_1)] complex in the

scum layer is higher by several times compared to that obtained in aqueous solution. This proves that the species is highly concentrated in the presence of HOL.
The [Cu(II)-(L_1)] complex in the scum layer exhibits bands at 250, 442 and 910 nm as shown at **Fig. 3c**.

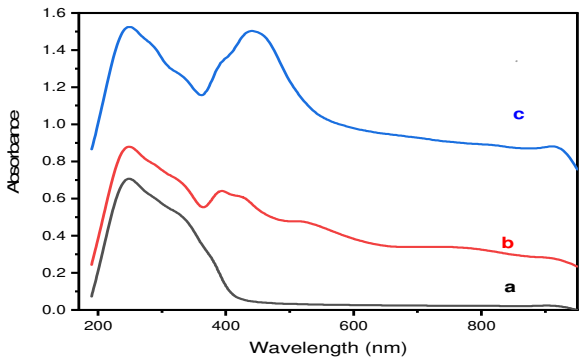

Figure 3: The electronic absorption spectra of (a) ligand L_1), (b) [Cu(II)-(L_1)] complex, (c) [Cu(II)-(L_1)] complex in the scum layer (HOL).

3.2.3. Elemental analysis

Table 3 shows the analytical results which demonstrate significant shifts in elemental composition during complexation. For the ligand(L_1).

Table 3: Elemental analysis for ligand(L_1), Cu(II) complex and Cu(II) complex in HOL (the scum layer).

Sample	C(%)	H(%)	N(%)	S(%)
Ligand	54.166	4.189	15.234	10.331
[Cu(II) -(L_1)]	37.037	3.680	12.531	8.812
[Cu(II) -(L_1)] in HOL	56.301	6.251	7.926	6.724

The most significant physical and micro analytical data collected for the ligand (L_1), along with its copper(II) Schiff base nano-complex (C_1) are illustrated in **Table 4.**

Table 4: Analytical and physical data of ligand L_1 and Cu(II) C_1 complex.

Parameters		**L_1**	**C_1**
Preparation method		Refluxing	Refluxing
Aspect		Crystal	Power
Color		Golden yellow	Deep brown
Reaction time		7h	6h
Melting point t(°C)		220	250
Yield %		86	99.1
Chemical formula		$C_{12}H_{11}N_3O_2S$	$C_{12}H_{10}N_3O_2SCuCl$
Characteristic infrared frequencies (cm^{-1})	ν(NH) $\nu(NH_2)$ ν(C=O) ν(C=N) ν(C=S) ν(C=C) ν(Cu–O) ν(Cu–N) ν(Cu–S)	3381 (3235-3147) 1711 1600 1362 3039 - - -	- (3570-3008) 1719 1608 1382 2924 597 535 483
UV - λ_{max} (nm)		249	249 and 394
Elemental analysis		C=54.166% N=15.234% H=4.189% S=10.331%	C=37.037% N=12.531% H=3.68% S=8.812%

3.2.4. Transmission electron micrograph (TEM)

The internal morphology of the [Cu(II) -(L_1)] complex was examined using transmission electron microscopy (TEM). **Fig. 4** reveals that [Cu(II)-(L_1)] complex was successfully synthesized in the nanoscale with a diameter ranging from 12.22 –20.94 nm.

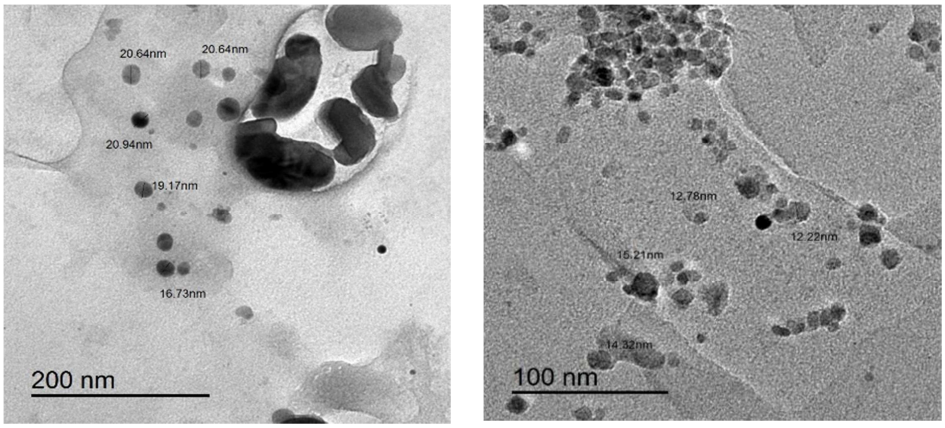

Figure 4: Transmission electron micrograph (TEM) of a cross section Cu(II) complex

3.3. DFT calculations

3.3.1. Optimized geometry

The optimized geometry of the ligand (L_1) and its corresponding [Cu(II)-(L_1)] Schiff base nano-complex are shown in **Fig. 5**.

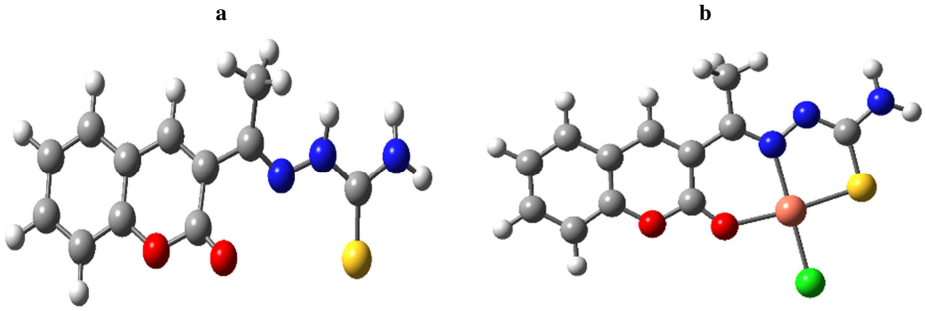

Figure 5: The optimized structures for the **(a)** ligand (L_1) and **(b)** copper complex [Cu(II)-(L_1] based on the DFT/ B3LYP/ DGDZVP methodology.

3.3.2. Molecular orbital properties and Global Reactivity Descriptors

The HOMO-LUMO gap can be used to determine the Global Reactivity Parameters [65–67] of a compound. **Fig. 6** illustrates the electron donor (HOMO) and electron acceptor (LUMO) sites for the ligand (L_1) and its [Cu(II)-(L_1)] Schiff base nano-complex. The optimized geometry of the ligand (L_1) and its [Cu(II)-(L_1)] Schiff base nano-complex are shown in **Fig. 5**. The HOMO and LUMO are shown in **Fig. 6** for the ligand (L_1) and its [Cu(II)-(L_1)] Schiff base nano-complex. From **Table 5**, the higher reactivity of the copper Schiff base nano-complex [Cu(II)-(L_1)] over the ligand (L_1) is explained in the light of the energy gap, ΔEgap, which measures the reactivity; as the energy gap decreases the reactivity increases. Also, the reactivity of the copper Schiff base nano-complex [Cu(II)-(L_1)] over the ligand (L_1) is cleared from the results of their ΔEgap and the amount of electronic charge transferring. As shown in **Table 5**, the ΔEgap for the [Cu(II)-(L_1)] Schiff base nano-complex exhibited greater reactivity compared to the ligand (L_1). Molecules with large energy gaps are considered hard, while those with small energy gaps are deemed soft [68, 69]. Soft molecules (σ) demonstrate higher reactivity than hard molecules (η) due to their lower ΔE(LUMO-HOMO) values. Consequently, hard molecules are less reactive in comparison to their soft counterparts. As seen from **Table 5** the [Cu(II)-(L_1)] Schiff base nano-complex is softer than the ligand (L_1). This confirms that the [Cu(II)-(L_1)] Schiff base nano-complex is more reactive than the ligand (L_1). Electronegativity (χ) quantifies an atom's capacity to draw electrons from other molecules [70]. When a ligand exhibits a high electronegativity value (χ), it demonstrates a strong ability to pull electrons from the [Cu(II)-(L_1)] Schiff base nano-complex. This enhanced electron attraction results in a more robust interaction, facilitating the formation of the compound.

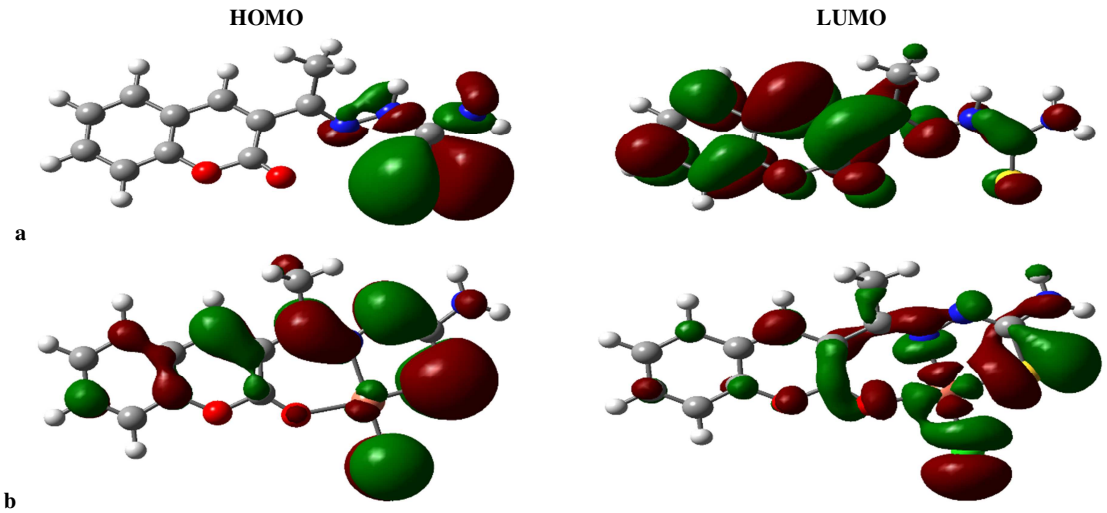

Figure 6: HOMO and LUMO structures for the **(a)** ligand (L_1) and **(b)** copper complex [Cu(II)-(L_1)], and based on the DFT/ B3LYP/ DGDZVP methodology.

The ionization potential; I_P and the electron affinity; E_A, can be expressed as negative values of E_{HOMO} and E_{LUMO}, respectively. The chemical reactivity of atoms and molecules can be characterized by their ionization energy. Atoms and molecules with higher ionization energy values tend to be more stable and chemically inert, while those with lower ionization energy are generally more reactive [71]. The ionization energy values for the molecules under investigation are presented in **Table 5**. The low ionization energy of the [Cu(II)-(L_1)] Schiff base nano-complex indicates their high reactivity than ligand (L_1). According to the definition electrophilicity index (ω) it measures the tendency of chemical species to acquire electrons. The results of electrophilicity seen in **Table 5** are in decreasing order; the [Cu(II)-(L_1)] Schiff base nano-complex > ligand (L_1). The dipole moment (μ) is another parameter that can shed light on molecular interactions. In the case of the [Cu(II)-(L_1)] Schiff base nano-complex, its dipole moment (μ) exceeds that of the ligand (L_1) alone. This increased value indicates enhanced interactions between the metal ion and the ligand (L_1) during the formation of the compound. The (E_{HOMO}), (E_{LUMO}), energy gap $\Delta E_{(LUMO-HOMO)}$, ionization potential (IP), electron affinity (EA), hardness (η), softness (σ), electronegativity (χ), chemical potential (μ), The Global electrophilicity index (ω) and dipole moment of the ligand (L_1) and its [Cu(II)-(L_1)] Schiff base nano-complex are illustrated in **Table 5**.

Table 5: The Global Reactivity Parameters determined using the DFT/ B3LYP/ DGDZVP methodology of calculations for the ligand (L_1) and **(b)** copper complex [Cu(II)-(L_1)].

Property	Ligand(L_1)	[Cu(II)-(L_1)]
E_{HOMO} [eV]	-0.21015	-0.22105
E_{LUMO} [eV]	-0.08898	-0.12013
ΔE_{gap} [eV]	0.12117	0.10092
η [eV]	0.060585	0.05046
σ [eV]$^{-1}$	16.50574	19.81768
I_p [eV]	0.21015	0.22105
E_A [eV]	0.08898	0.12013
χ [eV]	0.149565	0.17059
μ [eV]	-0.149565	-0.17059
ω [eV]	0.1846141	0.2883566
The dipole moment [Debye]	9.197	12.509

3.3.3. Theoretical Infra-red spectra analysis

Theoretical computations bolster infrared analyses, enabling reliable interpretation of experimental spectra from gaseous molecules. The most widely employed method for simulating IR spectra is the B3LYP/DGDZVP calculation approach. A comparison is drawn between IR spectra calculated for molecules in the gas phase and those measured in solid state. Additionally, Asadi et al. demonstrated a favorable correlation between gas phase DFT and experimental data from the

condensed phase [72]. **Fig. 7** displays the IR spectrum of the ligand (L_1) along with its [Cu(II)-(L_1)] Schiff base nano-complex.

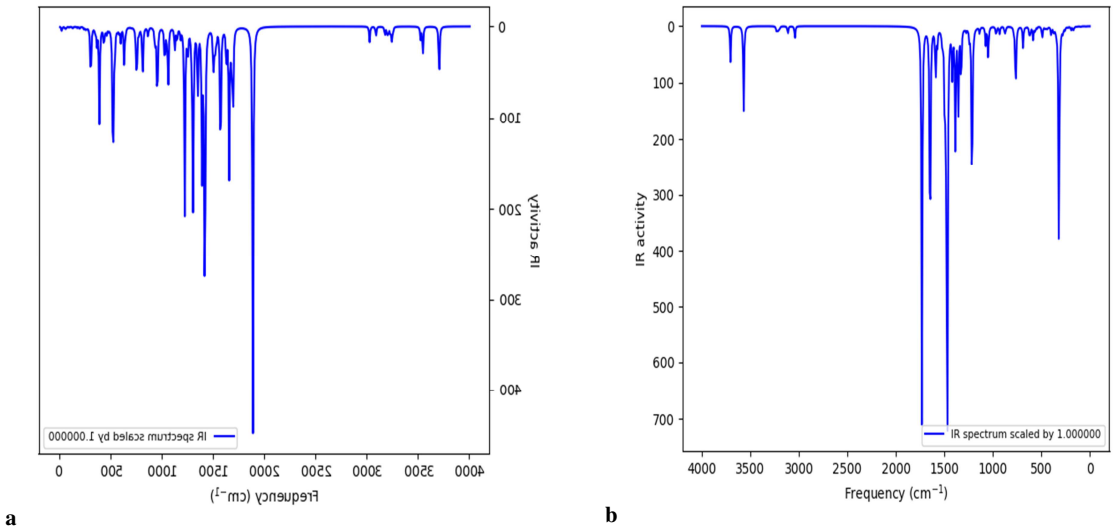

Figure 7: The calculated IR spectrum for the **(a)** ligand (L_1) and **(b)** copper complex [Cu(II)-(L_1)], and based on the DFT/ B3LYP/ DGDZVP methodology.

3.3.4. Molecular electrostatic potential (MEP)

Electrostatic potential (ESP) maps provide a visual representation of charge distribution across a molecule's surface. These three-dimensional representations, alternatively referred to as electrostatic potential energy maps or molecular electrical potential surfaces, showcase the partial charge distribution across a molecule's surface. By illustrating regions of varying charge intensity, ESP maps prove invaluable in determining molecular polarity and predicting intermolecular interactions, offering a visual analysis of charge distribution within these molecular systems. To enhance interpretability, a color gradient is employed, with red representing the lowest and blue indicating the highest electrostatic potential energy values. This color scheme effectively communicates the range of electrostatic potential energies across the molecular structure. **Fig. 8** presents the computed ESP maps for the ligand (L_1) and its corresponding [Cu(II)-(L_1)] Schiff base nano-complex.

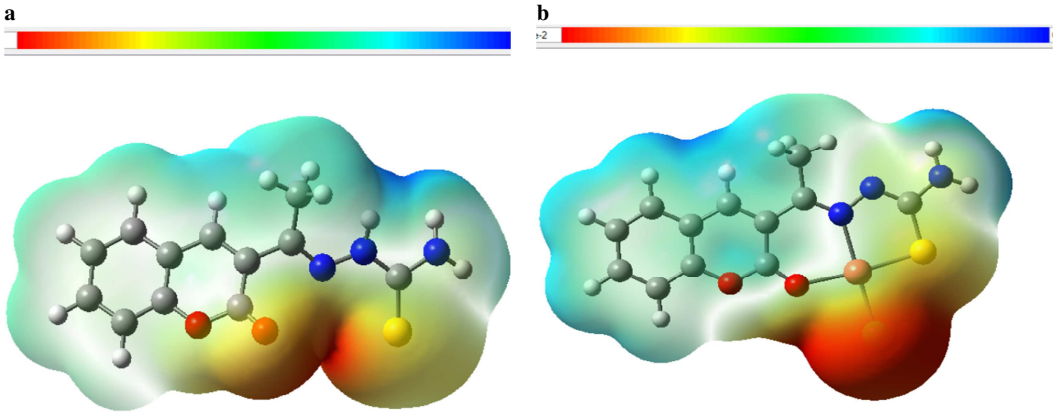

Figure 8: Electrostatic potential (ESP) surface maps visualization for the **(a)** ligand (L_1) and **(b)** copper complex [Cu(II)-(L_1)] based on the DFT/ B3LYP/ DGDZVP methodology. The spectrum from minimum to maximum levels of ESP is represented by the hues blue, green, and red. Minimum ESP surface areas are depicted as blue spheres, while maximum areas are shown as red spheres. Each image section contains a key that shows the corresponding ESP ranges.

3.4. Flotation-separation and FAAS determination of Cu(II) complex

3.4.1. Influence of pH

Among the key factors affecting the efficiency of analyte chelation and pre-concentration, the pH of the sample solution stands out as one of the most significant. An investigation was conducted to examine how pH influences the flotation of the complex in the presence and in the absence of Schiff base ligand (L_1) in the pH range (2 - 9) at room temperature using 7.87×10^{-5} molL^{-1} Cu(II) with 7.87×10^{-5} molL^{-1} of ligand and 2×10^{-4} molL^{-1} of HOL. The results are given in **Fig. 9**. In **Fig.**

9a, it was noticed that a maximum of 25% of the analyte was separated across all pH levels, which is considered analytically insufficient for Cu(II) flotation as Cu-oleate [73]. This led to multiple experiments aimed at achieving complete and selective Cu(II) separation using alternative organic collectors. Among these, the ligand (L_1) proved to be an outstanding collector. In **Fig. 9b** demonstrates the flotation efficiency reached its maximum (100%) at pH 5 in the presence of ligand (L_1). According to graphs (a) and (b), the effective role of the ligand (L_1) is clear; it forms a complex with Cu(II) ions rendering them more hydrophobic and easily separated from the solution bulk using the HOL surfactant. The observed decrease in absorbance under basic pH conditions was attributed to the formation of a white emulsion and to the formation of excessive foams of sodium oleate. This will hinder the reaction to complete [74].

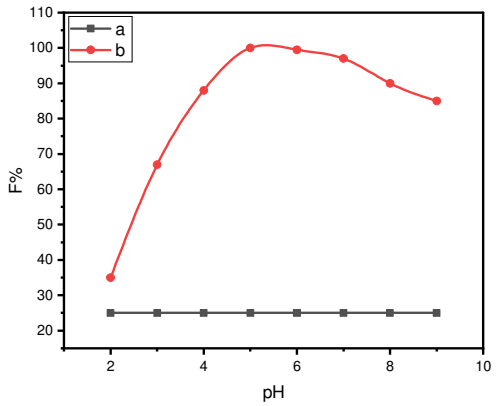

Figure 9: Effect of pH on flotation efficiency of 7.87×10^{-5} molL^{-1} Cu(II) **(a)** in absence of ligand (L_1), **(b)** in presence of ligand (L_1), using 2×10^{-4} molL^{-1} of HOL at room temperature.

3.4.2. Influence of ligand (L1)and metal concentration

The effect of ligand concentration on the flotation efficiency % of 7.88×10^{-5} molL^{-1} of Cu(II) at pH 5 was investigated by the addition of variable concentrations of L_1 using $2.0\text{x}10^{-4}$ molL^{-1} of HOL. From the results of **Fig. 10**, Cu(II) flotation efficiency was increased by increasing L_1 concentration in the range of (0.5-10) $\times10^{-5}$ molL^{-1}. The highest Cu(II) extraction efficiency was observed when the (L_1) concentration was 7.88×10^{-5} molL^{-1}, with a (Cu: L_1) ratio of (1:1). The F% remained stable as the Schiff base ligand concentration increased, which streamlines the process of analytically separating and detecting Cu(II), particularly in samples with unknown analyte quantities.

To validate these findings, additional experiments were conducted by altering the metal concentration. Complete separation was achieved up to the previously established (1:1) (Cu: L_1) ratio. Beyond this ratio, as Cu(II) increased, a slight decrease in separation percentage was observed. This indicates that there is insufficient ligand available for complete complexation and indirect separation.

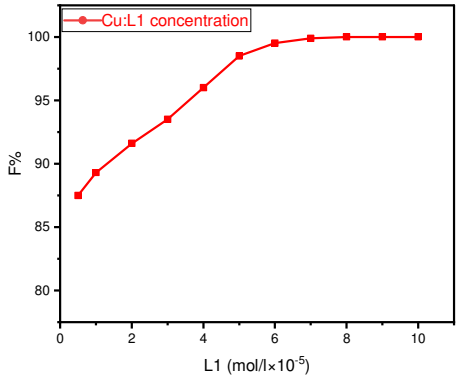

Figure 10: Influence of concentration of L_1 ligand on flotation effectiveness of 7.87×10^{-5} molL^{-1} Cu(II) at pH 5 using 2×10^{-4} molL^{-1} of HOL at ambient temperature.

3.4.3. Influence of HOL Concentration

The addition of a surfactant is generally employed to enhance the flotation of certain materials in aqueous solutions by rendering them hydrophobic. Hydrophobic substances can be more efficiently seeded from aqueous solutions compared to hydrophilic ones. These materials may include precipitates, complex ions, or ion associate (ion pairs) species. The concentration of HOL plays a crucial role; the separation percentage increases with higher surfactant concentrations up to a specific limit [75]. Experiments were conducted to examine the influence of HOL concentration on the floatability of 7.88×10^{-5} molL^{-1} of Cu(II) with 7.87×10^{-5} molL^{-1} of ligand at pH 5. **Fig. 11** illustrates that Cu(II) flotation efficiency reaches its peak and remains stable across a broad range of HOL concentrations from (2-7) x 10^{-4} molL^{-1}, before gradually declining. Consequently, a concentration of 2×10^{-4} molL^{-1} HOL was selected for all subsequent experimental procedures.

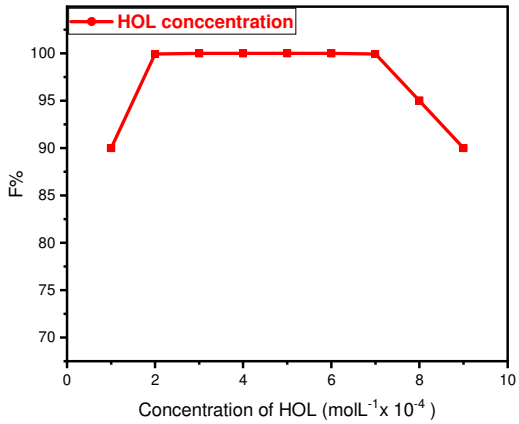

Figure 11: Influence of HOL concentration on the flotation effectiveness of 7.88×10^{-5} molL^{-1} Cu(II) in presence of 7.88×10^{-5} molL^{-1} of L_1 with pH 5 at ambient temperature.

3.4.4. Influence of different types of surfactants

To examine the effect of surfactant type on the flotation efficiency of 7.88×10^{-5} molL^{-1} Cu(II) in the presence of 7.88×10^{-5} molL$_{-1}$ of L_1 at pH 5, various surfactants were employed. As shown in **Table 6**, the Cu(II) flotation efficiency was tested using different surfactants including HOL, neutral Triton X-100, Triton X-114, Sodium lauryl sulphate, and cationic cetyltrimethylammonium bromide (CTAB). The results demonstrated that the flotation percentage (F%) of Cu(II) using HOL was approximately 100%. In contrast, nonionic surfactants such as TX-100 and TX-114, as well as cationic CTAB, produced abundant foam and created a substantial white scum layer on top of the aqueous phase. However, these surfactants failed to separate Cu(II), which remained in the solution. The F% of Cu(II) achieved with the other surfactants was less than 100%.

Table 6: Influence of different types of surfactants on the flotation effectiveness of 7.88×10^{-5} molL^{-1} Cu(II) in presence of 7.88×10^{-5} molL^{-1} of L_1 with pH 5 at ambient temperature.

Surfactant	F% of Cu(II)
HOL	100
Triton X-100	Foam, no flotation
Triton X-114	Foam, no flotation
CTAB	Foam, no flotation
Sodium lauryl sulphate	90

3.4.5. Influence of temperature

A thorough study was conducted to determine the ideal temperature for floating 7.88×10^{-5} molL^{-1} Cu(II) in the presence of 7.88×10^{-5} molL^{-1} of (L_1) at pH 5, utilizing 2×10^{-4} molL^{-1} of HOL within a temperature range of (10-80°C). The results depicted in **Fig. 12** indicate that temperature up to 60°C has no effect on the Cu(II) flotation efficiency. These results led researchers to conduct subsequent experiments at ambient temperature.

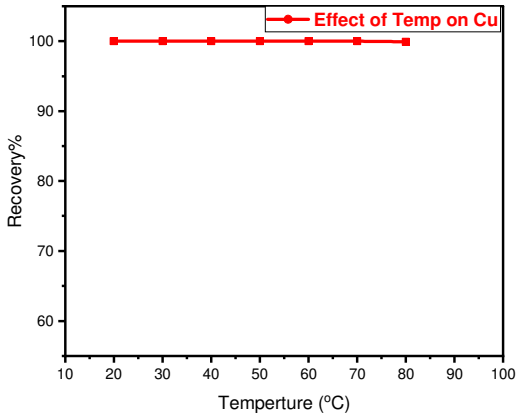

Figure 12: Influence of temperature on the flotation effectiveness of 7.88×10^{-5} molL^{-1} Cu(II) in presence of 7.88×10^{-5} molL^{-1} of L_1 using 2×10^{-4} molL^{-1} of HOL at pH 5.

3.4.6. Influence of shaking time

The time span between the introduction of all necessary components (Cu (II), ligand, HOL, and buffer) into the flotation cell and the commencement of flotation is referred to as flotation time. A study examining the effect of shaking time on Cu (II) flotation efficiency was performed within a (0-16) minute range under consistent conditions. As illustrated in **Fig. 13**, a brief 1-minute shaking time is adequate to achieve maximum flotation efficiency (100%) for the Cu(II) Schiff base nano-complex, with this efficiency remaining constant for up to 16 minutes. Consequently, a 2-minute shaking time was employed in subsequent experiments to ensure thorough Cu(II) separation. This finding highlights the rapid nature of the flotation separation method.

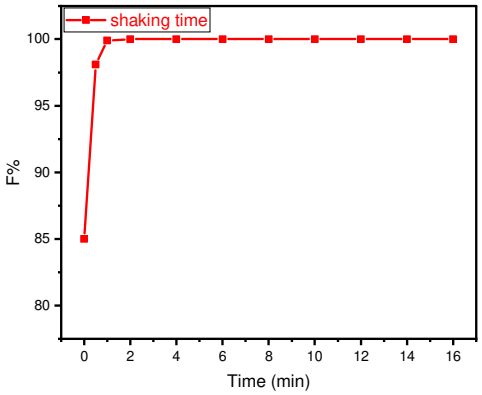

Figure 13: Influence of shaking time on the flotation effectiveness of 7.88×10^{-5} molL^{-1} Cu(II) in presence of 7.88×10^{-5} molL^{-1} of L_1 using 2×10^{-4} molL^{-1} of HOL with pH 5 at ambient temperature.

3.4.7. Influence of ionic strength

The study examined how different salt concentrations affected the flotation efficiency of 7.88×10^{-5} molL^{-1} Cu(II) when combined with 7.88×10^{-5} molL^{-1} of (L_1) and 2×10^{-4} molL^{-1} of HOL at pH 5. The selected salts for modifying ionic strength typically resemble those found in natural water samples. As demonstrated in **Table 7**, the addition of these salts did not significantly impact the flotation efficiency of the Cu(II) Schiff base nano-complex.

Table 7: Influence of ionic strength on the flotation effectiveness of 7.88×10^{-5} molL^{-1} Cu(II) in presence of 7.88×10^{-5} molL^{-1} of L_1 using 2×10^{-4} molL^{-1} of HOL with pH 5 at ambient temperature.

Salt	Concentration (M)	F%
		Cu(II)
NaCl	0.01	100
	0.05	100
	0.1	99.98

CH_3COONa	0.01 0.05 0.1	99.99 100 100
$Na_2S_2O_3$	0.01 0.05 0.1	100 99.98 100
KCl	0.01 0.05 0.1	100 100 100

3.4.8. Influence of volume

Multiple experiments were conducted to extract Cu(II) at a consistent concentration of 7.88×10^{-5} molL^{-1} from varying volumes of aqueous solutions. These extractions were performed using an appropriate laboratory instrument under the prescribed conditions. Hence, different volumes of a water sample (10 mL–1.5 L) and a constant volume of 2×10^{-4} molL^{-1} of HOL was chosen. flotation efficiency was not considerably affected up to 1 L (recovery >99%) using 5mL of oleic acid surfactant and reduced significantly as sample volume increased above 1.5 L as shown in **Fig. S3**. The ratio between the initial volume of analyte's solution and the resulting diluted surfactant-rich phase is termed the enrichment factor (preconcentration factor). Accordingly, this study has a preconcentration factor of 125 for Cu(II) under investigation [76].

3.4.9. Influence of foreign ions

Under optimal conditions, the impact of various foreign ion interferences on Cu(II) flotation efficiency was examined. The experiment utilized 7.88×10^{-5} molL^{-1} Cu(II) in the presence of 7.88×10^{-5} molL^{-1} (L_1), along with 2×10^{-4} molL^{-1} HOL at pH 5, conducted at ambient temperature. It occurred through the addition of known amounts of the investigated ions to the aqueous solution containing Cu(II) ion using the proposed methodology. The results indicate that some metal ions have no considerable effect on the Cu(II) response, while the influence of other foreign ions that have minimal interfering effects, was completely removed by enhancing the ligand's concentration as shown in **Table 8**.

The ligand (L_1) selectivity toward Cu(II) has been estimated through the [Cu(II)-(L_1)] complex stability constant calculation in the presence of various anions and cations, as shown in **Table 8**. The stability constant was calculated using **Eq. 3** [77].

$$K = [Cu - L_1]/[Cu]\,[L_1] \qquad (3)$$

In this equation, K represents the stability constant of the [Cu-(L_1)], while [Cu], [L_1], and [Cu-(L_1)] are the copper(II), ligand, and the formed complex concentrations, respectively.

It was observed that the [Cu-(L_1)] complex stability constant value was not significantly changed in the presence of the investigated anions and cations with a value of 4.1±0.01, which confirms the [Cu-(L_1)] complex stability in addition to the L_1 selectivity toward Cu(II) ions.

Table 8: Influence of foreign ions on the flotation effectiveness of7.88×10^{-5} molL^{-1} Cu(II) in presence of 7.88×10^{-5} molL^{-1} of L_1 using 2×10^{-4} molL^{-1} of HOL with pH 5 at ambient temperature. and stability constant of ligand (L_1) with different foreign ions.

Foreign ions	Cation/Anion (µg/ mL)	F % Cu(II)	Stability constant	
			[Cation-L_1] (Log K)	[Cu-L_1] (Log K)
-	-	100	-	4.103
Pb^{2+}	5	99.7	1.58	4.102
Co^{2+}	5	99.2	2	4.099
Mn^{2+}	5	99.3	1.95	4.100
Zn^{2+}	5	99.9	1.1	4.103
Cr^{3+}	5	99.65	1.65	4.102
Hg^{2+}	5	98	2.4	4.095
Cd^{2+}	5	99.9	1.1	4.103
Fe^{2+}	5	99.9	1.1	4.103
Al^{3+}	5	98.5	2.28	4.097
NO_3^-	310	99.4	---	4.100
$S_2O_3^{2-}$	560	100	---	4.103
Na^+	230	100	0	4.103
K^+	390.9	100	0	4.103
Cl^-	177.5	99.9	---	4.103
CH_3COO^-	295	98.9	---	4.098

3.5. Analytical characteristics

Under the previous experimental conditions, calibration graphs were achieved by pre-concentration of the sample (10 mL), which contained the known amounts of analyte. Under the optimum conditions of 7.88×10^{-5} $molL^{-1}$ Cu(II) in presence of 7.88×10^{-5} $molL^{-1}$ of L_1 using 2×10^{-4} $molL^{-1}$ of HOL with pH 5 at ambient temperature, the calibration graphs of Cu(II) had good linearity within the bands of (1.0-9.0 µg /mL). The limit of detection (LOD= 3.3 SD/m) established three times (n = 3), is 0.052 µg/mL, and relative standard deviation (RSD%) is 0.3868. The analysis parameters of the suggested method are illustrated in **Table 9**.

Table 9: The analytical characteristics

Parameter	Cu(II)
Sample volume (mL)	10
Regression equation*	y=0.03457x + 0.00097
Correlation coefficient	0.99941
SD	0.0005447
RSD % (n=5)	0.3869
LOD (µg/mL)	0.052
LOQ(µg/mL)	0.156
Enrichment factor	5
Linear range (µg/mL)	1.0-9

3.6. Flotation mechanism

The plausible interaction between HOL surfactant and [Cu(II)-(L_1)] Schiff base nano-complex is schematically represented in **Fig. 14**. The nature of interaction between Cu(II) complex and oleic acid surfactant must be studied to approach the actual mechanism of flotation. The proposed mechanism may proceed by forming physical force or by forming a hydrogen bond between the hydrophilic part of HOL and the active sites in the Schiff base nano-complex or by interaction between oleic acid and the Schiff base nano-complex, formed in solution, through a coordinate bond forming a self-floatable species ([Cu(II)-(L_1)] -HOL). The suggested flotation mechanism of Cu(II) is based on the following points:

i. Cu(II) reacts with the Schiff base ligand (L_1) to form a 1:1 (Cu: L_1) complex in aqueous solution.
ii. The IR spectrum of ligand (L_1) (**Fig. 2a**) exhibits absorption bands at 3381, (3235- 3147), and 3039 cm^{-1} which can be recognized to the ν(NH),ν(NH_2), and ν(C=C), respectively. The sharp bands at 1711, 1600, and 1362 cm^{-1} which can be assigned to bands ν(C=O), ν(C=N), and ν(C=S), respectively. The IR spectrum from [Cu(II)-(L_1)] Schiff base nano-complex isolated from aqueous solution (**Fig. 2b**) with ligand, it was detected that the ligand manages as monobasic tridentate ligand, coordinating through ketonic oxygen, azomethine nitrogen through coordination bond, and thiolic sulfur through covalent bond while the carbonyl of lactone and $-NH_2$ remain free. (**Fig. 2c**) shows the IR spectrum of [Cu(II)-(L_1)] Schiff base nano-complex extracted from the surfactant layer. It reveals the appearance of characteristic HOL surfactant bands.
iii. The floated species display the same color as those obtained in aqueous solution.
iv. **Fig.12** demonstrates that elevating the temperature above 60 ºC has no effect on the flotation process indicating that the floated complex is not easily destroyed by heat.

These observations point to that the mechanism of flotation is proposed to be due to hydrogen bond formation between the COOH group of HOL and -N complex interaction. Therefore, the system ([Cu(II)-(L_1)] -HOL) becomes hydrophobic and floated with air bubbles to the scum layer (generated inside the flotation cell by slight shaking).

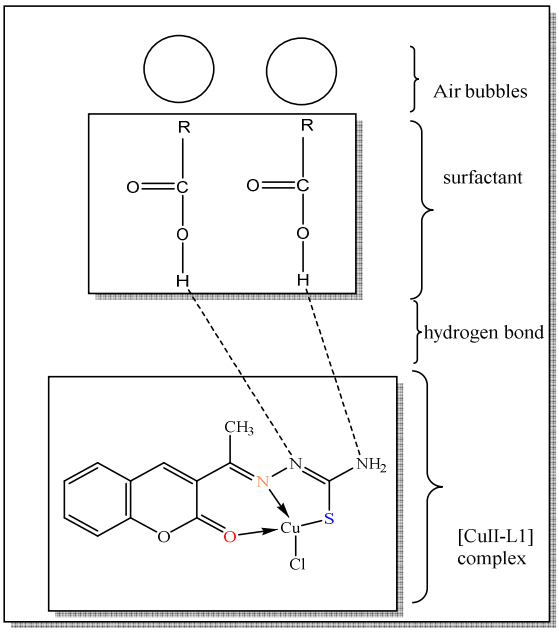

Figure 14: Mechanism of flotation of Cu(II) Schiff base nano-complex.

3.7. Applications

3.7.1. *natural water samples*

Many samples of water from various origins (distilled water, tap water, Nile water, and seawater) have been selected to detect the separation efficiency of the flotation method for the recovery of the analysts in these samples of water. After filtration of the water samples, the solutions (10 mL) containing the known concentration of the analyte were subjected to flotation procedures under the proposed conditions 7.88×10^{-5} molL^{-1} Cu(II) in presence of 7.88×10^{-5} molL^{-1} of L_1 using 2×10^{-4} molL^{-1} of HOL with pH 5 at ambient temperature. The flotation % of spiked water samples is more than 99%, and the RSD (n = 3) is less than 1% **(Table 10).**

Table 10: Recovery of Cu(II) in different water samples (n=3) after using 7.88×10^{-5} molL^{-1} of L_1 using 2×10^{-4} molL^{-1} of HOL at pH 5 at room temperature.

Types of water (location)	Spiked Cu(II) (µg/l)	Measured Cu(II) (µg/l)	F %	RSD %
Distilled Water (Our lab)	3.00 5.00 7.00	3.00 4.99 6.94	100 99.8 99.1	0.333 0.201 0.144
Tap Water (Our lab)	3.00 5.00 7.00	2.998 4.997 6.928	99.9 99.9 98.9	0.334 0.2 0.144
Nile Water (Mansoura city)	3.00 5.00 7.00	2.986 5.00 6.977	99.5 100 99.6	0.335 0.2 0.143
Sea Water (MarsaMatrouh city)	3.00 5.00 7.00	2.97 4.96 6.91	99 99.2 98.7	0.336 0.202 0.145

3.7.2. Application *on synthetic mixtures*

Various synthetic mixtures of 10 mL aqueous sample solution were prepared, containing different combinations of metal ions and analytes at known concentrations: 7.88×10^{-5} molL^{-1} of (L_1) using 2×10^{-4} molL^{-1} of HOL at pH 5 and ambient temperature. Flotation procedures were conducted under previously optimized conditions, and the flotation efficiency of the analytical substances was determined in the presence of varying concentrations of interfering ions using FAAS. The results presented in **Table 11** indicate that satisfactory recoveries were obtained for all analyses across all mixtures.

Table 11: Recovery of Cu(II) from synthetic mixtures (n=3) in the presence of 7.88×10^{-5} $molL^{-1}$ of L_1 using 2×10^{-4} $molL^{-1}$ of HOL with pH 5 at ambient temperature.

Synthetic mixtures composition (µg/l)	Concentration added of each (µg/ mL)	Cu(II) (µg/ mL)	
		Measured	R%
$Co^{2+} + Al^{3+}$	2.0	1.98	99
$Cd^{2+} + Hg^{2+}$	2.0	1.991	99.55
$Zn^{2+} + Pb^{2+}$	2.0	1.995	99.75
$Cd^{2+} + Co^{2+} + Al^{3+}$	3	2.92	97.3
$Zn^{2+} + Pb^{2+} + Hg^{2+}$	3	2.899	96.6
$Cd^{2+} + Co^{2+} + Al^{3+} + Hg^{2+}$	4	3.91	97.75
$Zn^{2+} + Pb^{2+} + Hg^{2+} + Co^{2+}$	4	3.90	97.5

3.7.3. Application on pharmaceutical samples

The proposed flotation procedure was successfully applied to investigate Cu(II) concentration in some copper containing pharmaceutical drugs. The results observed and illustrated in **Table 12**.

Table 12: Determination of Cu(II) in some pharmaceutical drug samples (n=3) in the presence of 7.88×10^{-5} $molL^{-1}$ of L_1 using 2×10^{-4} $molL^{-1}$ of HOL with pH 5 at ambient temperature.

Drug sample	Observed (µg/ mL)	Prepared (µg/ mL)	Measured	Recovery %	RSD, %
Vitastress	60	5	5	100	0.02
Totavit	18	5	4.85	97.8	0.021

3.8. Performance of the prepared Schiff base ligand (L_1)

In this study, a novel analytical method for determining copper concentration in water and pharmaceutical samples. This approach, combining ion flotation with flame atomic absorption spectroscopy (FAAS), utilized (L_1) and HOL surfactant compared to recently published methods. The comparison of all procedures and the same techniques used in current work and previous studies is noticeable that the analytical characteristics of this work were found to be more convenient in comparison with other papers as shown in **Table 13**.

Table 13: Comparative data from recent papers on preconcentration studies of Cu(II).

Method and instrumental detection	**LOD (µg/ mL)**	**RSD%**	**PF**	**Reference**
Flotation with (PTHAC)/FAAS	0.03	<3.72	200	[78]
Flotation with (PPKO)/AAS	0.7–0.8	<1	93	[79]
flotation with (BHABDI)/FAAS	1.7	2.1	125	[80]
SPE on activated carbon modified by dithiooxamide (rubeanic acid) / (FAAS)	0.5	<2	330	[81]
SPE with alpha-benzoin oxime followed by adsorption onto Diaion SP-850- solid phase extraction column/AAS	0.3	<8	50	[82]
CPE with (HPBTC)/FAAS	0.9	0.18	80	[83]
CPE with (MPDOC)/FAAS	0.5	<4	-	[84]
Flotation with Ligand(L_1)/FAAS	0.052	0.3869	125	This work

LOD: limit of detection, R.S.D.%: relative standard deviation, %PF: preconcentration factor, CPE: cloud point extraction, SPE: solid phase extraction,AAS: atomic absorption spectrometry.

3.9. Biological activity study

Heterocyclic Thiosemicarbazones are important because of their possible beneficial biological activity. Coumarin derivatives have been found to exhibit many useful applications, which include antibacterial, antifungal, antioxidant, analgesic, anticancer, anti-HIV, and anti-inflammatory [85]. Thiosemicarbazone derivatives have been the focus of medicinal chemists because of their potential biological activities. Therefore, it was aimed in the present investigation to synthesize and characterize newer coumarin thiosemicarbazone complex for their expected antimicrobial activities.

This investigation estimated the antimicrobial properties of a ligand and Cu(II) Schiff base nano-complex in the oleic layer against selected bacterial species such as gram negative (*Escherichia coli*) and gram positive (*Staphylococcus aureus*) which are provided and identified by Center of Genetic Engineering Biotechnology Mansoura University.

The antimicrobial activity of the ligand and [Cu(II)-(L_1)] Schiff base nano-complex was assessed against Gram-positive and Gram-negative bacteria using the agar well diffusion method. Each sample was prepared by dissolving 0.003 gm of sample powder in 1 mL of DMSO and Antibiotics were used are Amoxicillin (AX), Ciprofloxacin (CIP) and Gentamycin (GN) with *E. coli* and Ceftazidine (CAZ), Ampicillin, (A/S) and Cefotaxime (CTX) with *S. aureus* antibiotics to serve as an aid in comprehending the functional mechanism of our test materials and as a point of comparison. The biological activity of ligand(L_1) and Cu(II) Schiff base nano-complex against (a) *E. Coli* and (b) *S. aureus* is shown in **Fig. 15**. The values of the zone diameter corresponding to ligand (L_1), Cu(II) Schiff base nano-complex and antibiotics are presented in **Table 14**.

Analysis of the data provided in **Table 14** revealed that both L_1 and (Cu(II)-L_1)complex in HOL layer have antimicrobial activity against the Gm-ve*E. coli.* The inhibitory zone diameters of L_1 and C complex are 16 mm and 15mm which are greater than the standard AX antibiotic. Both L_1 and C complex had no antibacterial activity against the Gm +ve*S. aureus* strains.

Table 14: The values of the zone diameter corresponding to ligand(L_1), Cu(II) Schiff base nano-complex and antibiotics.

Samples / Bacterial strains	*Escherichia coli*		*Staphylococcus aureus*	
Ligand	16 mm		16 mm	
Cu(II) complex	15 mm		17 mm	
Antibiotics	AX	11 mm	CAZ	-ve
	GN	26 mm	CTX	18 mm
	Cip	38 mm	A/S	40 mm

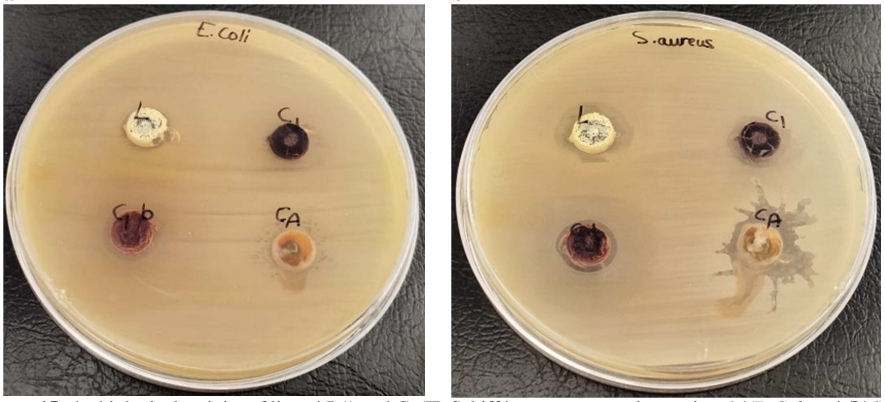

Figure 15: the biological activity of ligand(L1) and Cu(II) Schiff base nano-complex against **(a)***E. Coli* and **(b)***S. aureus*.

Table 15 represents the comparison of ligand (L_1) and [Cu(II)-(L_1)] results with other published thiosemicarbazone derivatives and their complexes. It can be noticed that (L_1) and [Cu(II)-(L_1)] showed comparable inhibition zones (mm) with the reported ligands and complexes, respectively.

Table 15: Comparative study on antibacterial activity of thiosemicarbazone derivatives or their complexes inhibition zone (mm)

Samples / Bacterial strains	Inhibition zone (mm)		Reference
	Escherichia coli	*Staphylococcus aureus*	
3-acetylcoumarin thiosemicarbazone (L_1)	16	16	This work
[Cu(II)-(L_1)]	15	17	This work
Coumarin-thiosemicarbazide hybrids ligand (SB-34)	7	-	[87]
Coumarin-thiosemicarbazide hybrids ligand (SB-35)	15	-	
Coumarin-thiosemicarbazide hybrids- Cu complex (38)	8	-	
Coumarin-thiosemicarbazide hybrids- Cu complex (41)	9	-	
Coumarin-thiosemicarbazide hybrids ligand (SB-45)	0	-	
Coumarin-thiosemicarbazide hybrids ligand (SB-46)	9	-	
Coumarin-thiosemicarbazide hybrids- Cu complex (49)	6	-	
Coumarin-thiosemicarbazide hybrids- Cu complex (52)	9	-	
(1E)-1-(1-(2-oxo-2H-chromen-3-yl)ethylidene)thiosemicarbazide (OCET)	16	17	[88]
$[Cu(OCET)_2]Cl_2H_2O$	13	12	

(1E)-1-(1-(6-bromo-2-oxo-2H-chromen-3-yl)ethylidene)thiosemicarbazide (BOCET)	17	17	
$[Cu(BOCET)_2(H_2O)2]Cl_2H_2O$	17	15	
(E)-2-(1-(2-oxo-2H-chromen-3-yl)ethylidene)-N-phenylhydrazine-1-carbothioamide (L_2)	16	22	[89]

4. Conclusion

The Schiff base ligand 3-acetyl coumarin thiosemicarbazone(L_1) was used to separate and preconcentrate Cu(II) from aqueous solutions. The ligand (L_1), along with its copper(II) Schiff base nano-complex were characterized by Fourier transform infrared spectroscopy (FTIR), Transmission electron microscopy, Ultraviolet-Visible spectroscopy (UV–Vis), elemental analysis and (TEM). This method employed flotation technique with oleic acid (HOL) serving as a surfactant. Findings demonstrated that the coordination between the metal ion and the ligand occurred through ketolate, azomethine, and thiolate groups of the ligand ligand(L_1). These results confirmed successful separation of 7.88×10^{-5} $molL^{-1}$ Cu(II) in presence of 7.88×10^{-5} $molL^{-1}$ of L_1 using 2×10^{-4} $molL^{-1}$ of oleic acid (HOL) serving as a surfactant HOL at pH 5 at room temperature. in various aquatic samples. The Cu(II) ion achieved 100% floatability. This study presents an environmentally sustainable approach for trace metal preconcentration and determination in water samples and pharmaceutical drugs. Mechanism of flotation was elucidated and found that the interactions between the complex and HOL was physical interactions. The mechanism of the antibacterial effect of the Schiff base nano-complex was elucidated. Furthermore, (DFT) were conducted to investigate the host-guest interactions between the ligand (L_1) and its copper(II) Schiff base nano-complex. The results show that the flotation preconcentration process is efficient, rapid, and economical method to extract and preconcentrate Cu(II) ion.

5. References

[1] Mostafa, A. G., El-Mekabaty, A., Hashem, M. A., & Akl, M. (2021). Selective Separation of Cu (II) from A single Metal Ion Solution by Using O-amino thiophenol-modified flax fiberd. Egyptian Journal of Chemistry, 64(4), 1701-1708.

[2] Akl, M. A., & Alharawi, W. S. (2018). A green and simple technique for flotation and spectrophotometric determination of cobalt (II) in pharmaceutical and water samples. Egyptian Journal of Chemistry, 61(4), 639-650.

[3] Otero-Calvis, A., Ramírez-Serrano, B., & Coello-Velázquez, A. (2020). Selectivity in the flotation of copper with xanthate over other ions present in wastewater: An experimental and computational study. Journal of Molecular Graphics and Modelling, 98, 107587.

[4] Akl, M. A., El-Zeny, A. S., Hashem, M. A., & El-Gharkawy, E. S. R. (2021). Synthesis, characterization and analytical applications of chemically modified cellulose for remediation of environmental pollutants. Egyptian Journal of Chemistry, 64(7), 3889-3901.

[5] Akl, M. A., Bekheit, M. M., & Salih, Q. M. (2015). Surfactant Assisted Separation-Spectrophotometric Procedure for the Trace Analysis of Copper (II) in Drug and Water Samples Using a Heterocyclic Pyridyl Azo Dye. Pharm Anal Acta, 6, 421.

[6] Khalifa, M. E., Akl, M. A., & Ghazy, S. E. S. (2001). Selective flotation-spectrophotometric determination of trace copper (II) in natural waters, human blood and drug samples using phenanthraquinone monophenylthiosemicarbazone. Chemical and pharmaceutical bulletin, 49(6), 664-668.

[7] Bidabadi, M. S., Dadfarnia, S., & Shabani, A. M. H. (2009). Solidified floating organic drop microextraction (SFODME) for simultaneous separation/preconcentration and determination of cobalt and nickel by graphite furnace atomic absorption spectrometry (GFAAS). Journal of hazardous materials, 166(1), 291-296.

[8] Jiang, H., Qin, Y., & Hu, B. (2008). Dispersive liquid phase microextraction (DLPME) combined with graphite furnace atomic absorption spectrometry (GFAAS) for determination of trace Co and Ni in environmental water and rice samples. Talanta, 74(5), 1160-1165.

[9] Matsumiya, H., Kageyama, T., & Hiraide, M. (2004). Multielement preconcentration of trace heavy metals in seawater with an emulsion containing 8-quinolinol for graphite-furnace atomic absorption spectrometry. Analytica chimica acta, 507(2), 205-209.

[10] Jankowski, K., Yao, J., Kasiura, K., Jackowska, A., & Sieradzka, A. (2005). Multielement determination of heavy metals in water samples by continuous powder introduction microwave-induced plasma atomic emission spectrometry after preconcentration on activated carbon. Spectrochimica Acta Part B: Atomic Spectroscopy, 60(3), 369-375.

[11] Cerutti, S., Moyano, S., Marrero, J., Smichowski, P., & Martinez, L. D. (2005). On-line preconcentration of nickel on activated carbon prior to its determination by vapor generation associated to inductively coupled plasma optical emission spectrometry. Journal of Analytical Atomic Spectrometry, 20(6), 559-561.

[12] Doner, G., & Ege, A. (2005). Determination of copper, cadmium and lead in seawater and mineral water by flame atomic absorption spectrometry after coprecipitation with aluminum hydroxide. Analytica Chimica Acta, 547(1), 14-17.

[13] Sulejmanović, J., Memić, M., Šehović, E., Omanović, R., Begić, S., Pazalja, M., ... & Sher, F. (2022). Synthesis of green nano sorbents for simultaneous preconcentration and recovery of heavy metals from water. Chemosphere, 296, 133971.

[14] Akl, M. A., El-Zeny, A. S., Hashem, M. A., El-Gharkawy, E. S. R., & Mostafa, A. G. (2023). Flax fiber based semicarbazide biosorbent for removal of Cr (VI) and Alizarin Red S dye from wastewater. Scientific Reports, 13(1), 8267.

[15] Yang, Z., Ma, J., Liu, F., Zhang, H., Ma, X., & He, D. (2022). Mechanistic insight into pH-dependent adsorption and coprecipitation of chelated heavy metals by in-situ formed iron (oxy) hydroxides. Journal of Colloid and Interface Science, 608, 864-872.
[16] Serage, A. A., Mostafa, M. M., & Akl, M. A. (2022). Low Cost Agro-Residue Derived Biosorbents: Synthesis, Characterization and Application for Removal of Lead Ions ffrom Aqueous Solutions. Egyptian Journal of Chemistry, 65(131), 447-461.
[17] Akl MA, Hashem MA, Mostafa AG. Synthesis, characterization, antimicrobial and photocatalytic properties of nano-silver-doped flax fibers. Polymer Bulletin. 2022;
[18] Akl MA, El-Zeny AS, Hashem MA, ElGharkawy ESRH. Synthesis, Characterization and Analytical Applications of Chemically Modified Cellulose for Remediation of Environmental Pollutants. Egypt J Chem. 2021 Jul 1;64(7):3889–901.
[19] Akl, M. A., Hashem, M. A., Ismail, M. A., & Abdelgalil, D. A. (2022). Novel diaminoguanidine functionalized cellulose: synthesis, characterization, adsorption characteristics and application for ICP-AES determination of copper (II), mercury (II), lead (II) and cadmium (II) from aqueous solutions. BMC chemistry, 16(1), 65.
[20] Saleh MO, Hashem MA, Akl MA. Removal of Hg (II) metal ions from environmental water samples using chemically modified natural sawdust. Egypt J Chem. 2021 Feb 1;64(2):1027–34.
[21] Akl, M. A., Bekheit, M. M., & Helmy, I. (2016). Application of CPE-FAAS methodology for the analysis of trace heavy metals in real samples using phenanthraquinone monophenyl thiosemicarbazone and triton X-114. J Anal Bioanal Tech, 7(325), 2.
[22] Nour, M., AbdElaal, M., & Akl, M. A. (2023). Efficient CPE-ICP OES Determination of Palladium (II) in Environmental Samples Using Schiff Base Ligand and Triton X-114. Egyptian Journal of Chemistry, 66(12), 455-466.
[23] Saad, H. E., Sheta, S. M., Akl, M. A., & El-Gharkawy, E. S. R. (2024). Determination of Co (II) and Pd (II) by inductivity coupled plasma–atomic emission spectrometry after extraction from water and pharmaceutical samples by cloud point extraction. Essential Chem, 1(1), 1-12.
[24] Sarrafi, A., Rahmati, B., Hassani, H. R., & Shirazi, H. H. A. (2004). Recovery of copper from reverberatory furnace slag by flotation. Minerals Engineering, 17(3), 457-459.
[25] Akl, M. A., El-Asmy, A. A., & Yossef, W. M. (2005). Separation via flotation, spectrophotometric speciation, and determination of vanadium (IV) in wastes of power stations. Analytical sciences, 21(11), 1325-1335.
[26] Ghazy, S. E., & Kabil, M. A. (1994). Determination of trace copper in natural waters after selective separation by flotation. Bulletin of the Chemical Society of Japan, 67(8), 2098-2102.
[27] Akl, M. A., Isamil, D. S., Jeragh, B., & El-Asmy, A. A. (2014). Flotation separation and spectrophotometric determination of Sc3+ in certified materials and different water resources. Journal of Scientific Research and Reviews, 3, 008-017.
[28] Akl, M. A., & Masoud, R. (2018). Flotation and enhanced spectrophotometric determination of uranium (VI) in environmental samples. Egyptian Journal of Chemistry, 61(2), 337-348.
[29] Polat, H., & Erdogan, D. (2007). Heavy metal removal from waste waters by ion flotation. Journal of Hazardous Materials, 148(1-2), 267-273.
[30] Akl, M. A., Kabil, M. A. G., Abdallah, A. M., & Ismael, D. S. (2003). Flotation and spectrophotometry: Thorough investigation and application to the determination of the total amounts of lanthanum and yttrium in natural samples. Bulletin of the Chemical Society of Japan, 76(8), 1543-1547.
[31] More, M. S., Joshi, P. G., Mishra, Y. K., & Khanna, P. K. (2019). Metal complexes driven from Schiff bases and semicarbazones for biomedical and allied applications: a review. Materials Today Chemistry, 14, 100195.
[32] Hoult, J. R. S., & Payá, M. (1996). Pharmacological and biochemical actions of simple coumarins: natural products with therapeutic potential. General Pharmacology: The Vascular System, 27(4), 713-722.
[33] Hussein, M. A., Iqbal, M. A., Asif, M., Haque, R. A., Ahamed, M. B. K., Majid, A. M. A., & Guan, T. S. (2015). Asynthesis, crystal structures and in vitro anticancer studies of new thiosemicarbazone derivatives. Phosphorus, Sulfur, and Silicon and the Related Elements, 190(9), 1498-1508.
[34] Yenial, Ü., & Bulut, G. (2017). Examination of flotation behavior of metal ions for process water remediation. Journal of Molecular Liquids, 241, 130-135.
[35] Nongpiur, C. G. L., Soh, C., Diengdoh, D. F., Verma, A. K., Gogoi, R., Banothu, V., ... & Kollipara, M. R. (2023). 3-acetyl-coumarin-substituted thiosemicarbazones and their ruthenium, rhodium and iridium metal complexes: An investigation of the antibacterial, antioxidant and cytotoxicity activities. Journal of Organometallic Chemistry, 998, 122788.
[36] Pangal, A., Shaikh, J. A., Muiz, G., Mane, V., & Ahmed, K. (2013). Novel 3-acetylcoumarin Schiff's base synthesis from different acid hydrazide. Int. Res. J. Pharm, 4(10), 108-110.
[37] Akl, M. A., Bekheit, M. M., & Salih, Q. M. (2015). Surfactant Assisted Separation-Spectrophotometric Procedure for the Trace Analysis of Copper (II) in Drug and Water Samples Using a Heterocyclic Pyridyl Azo Dye. Pharm Anal Acta, 6, 421.
[38] Becke, A. D. (1992). Density-functional thermochemistry. I. The effect of the exchange-only gradient correction. The Journal of chemical physics, 96(3), 2155-2160.
[39] H.Y. Ammar and E. R. H. El-Gharkawy, European Journal of Scientific Research, Vol.120 No.3 (2014), pp.401-415.
[40] El-Gharkawy, E. S. R., & Ammar, H. Y. (2018). Adsorption of CO on TM-deposited (MgO) 12 nano-Cage (TM= Ni, Pd and Pt): a study on electronic properties. Journal of Nanoelectronics and Optoelectronics, 13(4), 546-553.

[41] Sheta, S. M., Abd-Elzaher, M. M., & El-Sheikh, S. M. (2021). A novel nano-lanthanum complex: synthesis, characterization and application as a macrofuran chemosensor in pharmaceutical, biological and environmental samples. RSC advances, 11(16), 9675-9681.
[42] Akl, M. A., El-Gharkawy, E. S. R., El-Mahdy, N. A., El-Sheikh, S. M., & Sheta, S. M. (2020). A novel nano copper complex: potentiometry, DFT and application as a cancer prostatic biomarker for the ultrasensitive detection of human PSA. Dalton Transactions, 49(44), 15769-15778.
[43] Abd El-Maksoud, S. A., El-Dossoki, F. I., Migahed, M. A., Gouda, M. M., & El-Gharkawy, E. S. R. (2021). New Imidazol-1-ium Bromide derivative surfactants as corrosion inhibitors for carbon steel in 1 M HCl solutions: Experimental and theoretical studies. Journal of Bio-and Tribo-Corrosion, 7, 1-15.
[44] Akl, M. A., El-Mahdy, N. A., & El-Gharkawy, E. S. R. (2022). Design, structural, spectral, DFT and analytical studies of novel nano-palladium schiff base complex. Scientific Reports, 12(1), 17451.
[45] Godbout, N., Salahub, D. R., Andzelm, J., & Wimmer, E. (1992). Optimization of Gaussian-type basis sets for local spin density functional calculations. Part I. Boron through neon, optimization technique and validation. Canadian Journal of Chemistry, 70(2), 560-571.
[46] Sosa, C., Andzelm, J., Elkin, B. C., Wimmer, E., Dobbs, K. D., & Dixon, D. A. (1992). A local density functional study of the structure and vibrational frequencies of molecular transition-metal compounds. The Journal of Physical Chemistry, 96(16), 6630-6636.
[47] Frisch, M., & Clemente, F. MJ Frisch, GW Trucks, HB Schlegel, GE Scuseria, MA Robb, JR Cheeseman, G. Scalmani, V. Barone, B. Mennucci, GA Petersson, H. Nakatsuji, M. Caricato, X. Li, HP Hratchian, AF Izmaylov, J. Bloino and G. Zhe, Gaussian, 9.
[48] O'boyle, N. M., Tenderholt, A. L., & Langner, K. M. (2008). Cclib: a library for package-independent computational chemistry algorithms. Journal of computational chemistry, 29(5), 839-845.
[49] Weinhold, F., Landis, C. R., & Glendening, E. D. (2016). What is NBO analysis and how is it useful?. International reviews in physical chemistry, 35(3), 399-440.
[50] Dennington, R., Keith, T., & Millam, J. (2009). Semichem Inc. Shawnee Mission KS, GaussView, Version, 5(8).
[51] Shoba, D., Periandy, S., Karabacak, M., & Ramalingam, S. (2011). Vibrational spectroscopy (FT-IR and FT-Raman) investigation, and hybrid computational (HF and DFT) analysis on the structure of 2, 3-naphthalenediol. Spectrochimica Acta Part A: Molecular and Biomolecular Spectroscopy, 83(1), 540-552.
[52] Koopmans, T. (1934). Über die Zuordnung von Wellenfunktionen und Eigenwerten zu den einzelnen Elektronen eines Atoms. physica, 1(1-6), 104-113.
[53] Wang, H., Wang, X., Wang, H., Wang, L., & Liu, A. (2007). DFT study of new bipyrazole derivatives and their potential activity as corrosion inhibitors. Journal of Molecular Modeling, 13, 147-153.
[54] Pauling, L. (1960). The nature of the chemical bond and the structure of molecules and crystals: an introduction to modern structural chemistry (Vol. 18). Cornell university press.
[55] Senet, P. (1997). Chemical hardnesses of atoms and molecules from frontier orbitals. Chemical physics letters, 275(5-6), 527-532.
[56] Parr, R. G., Szentpály, L. V., & Liu, S. (1999). Electrophilicity index. Journal of the American Chemical Society, 121(9), 1922-1924.
[57] Chattaraj, P. K., & Roy, D. R. (2007). Update 1 of: electrophilicity index. Chemical reviews, 107(9), PR46-PR74.
[58] Gómez, B., Likhanova, N. V., Domínguez-Aguilar, M. A., Martínez-Palou, R., Vela, A., & Gazquez, J. L. (2006). Quantum chemical study of the inhibitive properties of 2-pyridyl-azoles. The Journal of Physical Chemistry B, 110(18), 8928-8934.
[59] Murray, R.; Rosenthal, S.; Kobayashi, S.; Pfaller, A. (1998). Medical Microbiology. 3rd ed. St. Louis: Mosby, p.161.
[60] Sardari, A.; Gholamreza, M.; Daneshtalab, M. (1998). Phytopharmaceuticals. Part 1: Antifungal Activity of Selected Iranian and Canadian Plants. Pharm. Biol., 36:180-188
[61] Hasanen, J. A. (2012). Synthesis and mass spectra of some new 3-substituted coumarin derivatives. Der PharmaChemica, 4(5), 1923-1934.
[62] Kumar, R., Sharma, S., Singh, R. V., & Rastogi, S. (2013). Synthesis, Characterization and biological evaluation of niobium (v) complexes of coumarin based imines. Rasayan Journal of Chemistry, 6, 183-189.
[63] Ibarra, J., Melendres, J., Almada, M., Burboa, M. G., Taboada, P., Juárez, J., & Valdez, M. A. (2015). Synthesis and characterization of magnetite/PLGA/chitosan nanoparticles. Materials Research Express, 2(9), 095010.
[64] Zhang, L., He, R., & Gu, H. C. (2006). Oleic acid coating on the monodisperse magnetite nanoparticles. Applied Surface Science, 253(5), 2611-2617.
[65] Praveen, P. L., DS, R., & Ojha, D. P. (2017). UV spectral characterization of a smectic-C liquid crystal: Theoretical support to the experiment. Molecular Crystals and Liquid Crystals, 643(1), 76-82.
[66] Veligeti, R., Ramakrishna, D. S., Madhu, R. B., & Anireddy, J. S. (2022). Synthesis of fluoro and trifluoromethyl substituents containing novel tetracyclic N-benzylated benzopiperazine fused acridone regioisomers using a greener solvent 2-MeTHF and their DFT studies. Journal of Fluorine Chemistry, 257, 109989.
[67] Veligeti, R., Anireddy, J. S., Madhu, R. B., & Ramakrishna, D. S. (2022). One pot, three component synthesis of fluoro and trifluoromethyl substituted unsymmetrical dihydropyrazine fused acridine-3-carboxamide using renewable 2-MeTHF solvent and their DFT studies. Journal of Fluorine Chemistry, 261, 110019.
[68] Pearson, R. G. (1993). The principle of maximum hardness. Accounts of Chemical Research, 26(5), 250-255.
[69] Reed, A. E., Curtiss, L. A., & Weinhold, F. (1988). Intermolecular interactions from a natural bond orbital, donor-acceptor viewpoint. Chemical Reviews, 88(6), 899-926.

[70] Parr, R. G., Donnelly, R. A., Levy, M., & Palke, W. E. (1978). Electronegativity: the density functional viewpoint. The Journal of chemical physics, 68(8), 3801-3807.
[71] Chakraborty, T., Gazi, K., & Ghosh, D. C. (2010). Computation of the atomic radii through the conjoint action of the effective nuclear charge and the ionization energy. Molecular Physics, 108(16), 2081-2092.
[72] Asadi, Z., Esrafili, M. D., Vessally, E., Asnaashariisfahani, M., Yahyaei, S., & Khani, A. (2017). A structural study of fentanyl by DFT calculations, NMR and IR spectroscopy. Journal of Molecular Structure, 1128, 552-562.
[73] Lemlich, R. (Ed.). (2012). Adsorptive bubble separation techniques. Elsevier.
[74] Akl, M. A., Mostafa, M. M., & Elbadrawy, Z. (2014). Separation via flotation and spectrometric determination of copper (II) in environmental samples using a newly synthesized girard T derivative. Chem Sci J, 5, 087.
[75] Akl, M. A., Alharwi, W. S., & El-Sokkary, A. (2023). Fe (III)-Morin complex: DNA interaction studies, speciation, flotation and spectrometric determination of iron (III) in media of diverse origin. Egyptian Journal of Chemistry, 66(5), 413-424.
[76] El Sheikh, R., Shaltout, M., El Nabawy, K., & A Gouda, A. (2020). A green enrichment method of copper, manganese and nickel in water samples via cloud point extraction. Analytical and Bioanalytical Chemistry Research, 7(1), 49-60.
[77] Kiani-anboui, R., & Ghasemi, M. H. (2022). A QSPR Study for the Prediction of the Selectivity of Pb (II) Sensors by Stability Constants of Ion-Ionophore Complexes. Analytical and Bioanalytical Electrochemistry, 14(6), 598-609.
[78] Akl, M. A., Mostafa, M. M., & Elbadrawy, Z. (2014). Separation via flotation and spectrometric determination of copper (II) in environmental samples using a newly synthesized girard T derivative. Chem Sci J, 5, 087.
[79] Karimi, H., Ghaedi, M., Shokrollahi, A., Rajabi, H. R., Soylak, M. U. S. T. A. F. A., & Karami, B. (2008). Development of a selective and sensitive flotation method for determination of trace amounts of cobalt, nickel, copper and iron in environmental samples. Journal of hazardous materials, 151(1), 26-32.
[80] Ghaedi, M., Shokrollahi, A., Montazerozohori, M., Marahel, F., & Soylak, M. (2010). Development of a flotation method for preconcentration-separation of trace amounts of some metal ions in plant tissues prior to their FAAS determinations. Quimica Nova, 33, 404-410.
[81] Ghaedi, M., Ahmadi, F., & Soylak, M. U. S. T. A. F. A. (2007). Preconcentration and separation of nickel, copper and cobalt using solid phase extraction and their determination in some real samples. Journal of Hazardous Materials, 147(1-2), 226-231.
[82] Soylak, M., & Tuzen, M. (2006). Diaion SP-850 resin as a new solid phase extractor for preconcentration-separation of trace metal ions in environmental samples. Journal of Hazardous Materials, 137(3), 1496-1501.
[83] Akl, M. A., AL-Rabasi, A., & Molouk, A. F. (2021). Cloud point extraction and FAAS determination of copper (II) at trace level in environmental samples using N-benzamido-N'-benzoylthiocarbamide and CTAB. Egyptian Journal of Chemistry, 64(1), 313-322.
[84] Snigur, D. V., Dubovyi, V. P., & Chebotarev, A. N. (2020). Atomic-absorption determination of copper (II) in water samples after its cloud-point extraction preconcentration. Moscow University Chemistry Bulletin, 75, 328-332.
[85] Vekariya, R. H., Patel, K. D., Rajani, D. P., Rajani, S. D., & Patel, H. D. (2017). A one pot, three component synthesis of coumarin hybrid thiosemicarbazone derivatives and their antimicrobial evolution. Journal of the Association of Arab Universities for Basic and Applied Sciences, 23, 10-19.
[86] Ceramella, J., Iacopetta, D., Catalano, A., Cirillo, F., Lappano, R., & Sinicropi, M. S. (2022). A review on the antimicrobial activity of Schiff bases: Data collection and recent studies. Antibiotics, 11(2), 191.
[87] Sharma, A., Devi, S., & Kumar, S. (2024). A review on synthesis of coumarin derived Schiff's base metal complexes and their control over *E. coli* bacterium. Main Group Chemistry, 23(3), 299-327.
[88] Refat, M. S., El-Deen, I. M., Anwer, Z. M., & El-Ghol, S. (2009). Bivalent transition metal complexes of coumarin-3-yl thiosemicarbazone derivatives: Spectroscopic, antibacterial activity and thermogravimetric studies. Journal of Molecular structure, 920(1-3), 149-162.
[89] Nongpiur, C. G. L., Soh, C., Diengdoh, D. F., Verma, A. K., Gogoi, R., Banothu, V., ... & Kollipara, M. R. (2023). 3-acetyl-coumarin-substituted thiosemicarbazones and their ruthenium, rhodium and iridium metal complexes: An investigation of the antibacterial, antioxidant and cytotoxicity activities. Journal of Organometallic Chemistry, 998, 122788.